Journal of Materials Chemistry A

Accepted Manuscript

ROYAL SOCIETY OF CHEMISTRY

www.rsc.org/materialsA

A Comparative Study on the Oxidation State of Lattice Oxygen among $Li_{1.14}Ni_{0.136}Co_{0.136}Mn_{0.544}O_2$, Li_2MnO_3, $LiNi_{0.5}Co_{0.2}Mn_{0.3}O_2$ and $LiCoO_2$ for the Initial Charge-Discharge

Shaojie Han [a,b], Yonggao Xia [a,*], Zhen Wei[a], Bao Qiu[a], Lingchao Pan[a], Qingwen Gu[a], Zhaoping Liu [a,*],[1]Zhiyong Guo[b]

[a] *Ningbo Institute of Materials Technology and Engineering, Chinese Academy of Sciences, Zhejiang 315201, P. R. China.*

[b] *The School of Material Science and Chemical Engineering, Ningbo University, Zhejiang 315211, P. R. China*

Abstract: The Li-rich layered oxides are attractive electrode materials for their high reversible specific capacity (>250 mAh g^{-1}), however, the origin of their abnormal capacity is still ambiguous. In order to elucidate this curious anomaly, we make a comparison of lattice oxygen's oxidation states among Li-rich layered oxide $Li_{1.14}Ni_{0.136}Co_{0.136}Mn_{0.544}O_2$, Li_2MnO_3 and $LiNi_{0.5}Co_{0.2}Mn_{0.3}O_2$, the two components in Li-rich layered oxides, and the most common layered oxide $LiCoO_2$ before and after initial charge-discharge. For simplicity, we employ the chemical treatments of NO_2BF_4 and LiI acetonitrile solutions to simulate the electrochemical delithiation and lithiation processes. The X-ray photoelectron spectroscopy (XPS) studies reveal that part of lattice oxygen in $Li_{1.14}Ni_{0.136}Co_{0.136}Mn_{0.544}O_2$ and Li_2MnO_3 undergo a reversible redox process (possibly, $O^{2-} \leftrightarrow O_2^{2-}$) while in $LiNi_{0.5}Co_{0.2}Mn_{0.3}O_2$ and

* Corresponding authors. Tel./Fax: +86-574-8668-5096.
E-mail addresses: xiayg@nimte.ac.cn (Y. Xia), liuzp@nimte.ac.cn (Z. Liu).

$LiCoO_2$ do not, which indicates that the extra capacity of Li-rich layered oxides can be attributed to the reversible redox processes of oxygen in the Li_2MnO_3 component. The thermogravity analysis (TGA) experiments further suggest that the formed O_2^{2-} species in the delithiated $Li_{1.14}Ni_{0.136}Co_{0.136}Mn_{0.544}O_2$ can decompose into O_2 at about 210 °C. This phenomenon demonstrates a competitive relationship between extra capacity and thermal stability, which will be a big challenge in the practical applications of these materials.

Introduction

With the explosive growth of portable electronic devices, lithium-ion batteries (LIBs), the advanced chemical power sources, have been playing an increasing important role in the modern life. Since first commercialized by Sony in 1991, they have been received extensive attentions from both academia and industry.[1] However, the development of LIBs seems poor in the light of Moore's law in electronics (according to which memory capacity doubles every 18 months). The energy storage capability of LIBs is greatly determined by the cathode materials. Up to now, $LiCoO_2$ is still the main cathode material in the market. It is not sustainable as the low abundance of cobalt in nature, and its energy density is also failed to meet the demands of today's people. In order to expand the application of LIBs to the power-sources for the burgeoning electric vehicles (EVs), the development of new cathode materials with high performance and low-cost is imminent.

Among the positive electrode candidates studied at present, the Li-rich layered oxides are most attractive for the next generation LIBs due to their high reversible

specific capacities exceeding 250 mAh g^{-1},[2-7] which are two times larger than the current commercialized layered oxides,[8] spinels[9] or polyanionic compounds.[10] According to the previous reports, they are either as solid solutions $Li[Li_xM_{1-x}]O_2$[12-13] or as nanocomposite structures $xLi_2MnO_3 \cdot (1-x)LiMO_2$ (M = Mn, Ni, Co, etc.),[14-17] composed of monoclinic Li_2MnO_3 domains (*C2m*) and rhombohedral $LiMO_2$ domains (*R-3m*).

The high specific capacities of these compounds mainly come from the activation of Li_2MnO_3 component at about 4.5 V *vs.* Li^+/Li. During the initial charge process, the layered $LiMO_2$ component participates in the electrochemical reactions first while the Li_2MnO_3 component keeps electrochemically inactive.[18] Once charged to high potentials, typically above 4.4 V, the lithium-ions in the Li_2MnO_3 can be extracted and an irreversible long plateau can be observed at ~4.5 V.[19] It is believed that the Mn^{4+} is difficult to be further oxidized, so the charge compensation mechanism of the activation process is focused on the oxidation of lattice oxygen. Oxygen gas is considered to be lost from the material at the end of the charge as was previously observed by mass spectrometry, which induces a large irreversible capacity.[5,20-22] Here, Li_2MnO_3 component is considered to be transformed into a compound stoichiometrically similar to MnO_2 after initial charge.[23] The latter is electrochemical active during the cathodic process, in which Mn^{4+} can be reduced to Mn^{3+}, resulting in a structural transformation from layered to spinel. This process is also accompanied by the voltage fade.[24,25] However, the theoretical capacity calculated in this electrochemical reaction mechanism cannot reach the overall reversible capacity from

the actual charge and discharge process, especially at high temperature. Ohzuku *et al.*[26] detailed discussed the possible reaction mechanisms of $Li_{1.2}Ni_{0.2}Mn_{0.6}O_2$ showing the rechargeable capacity more than 300 mAh g^{-1}. They found that the initial irreversible capacity at 55 ^oC is only 40 mAh g^{-1}. It is much smaller than the expected irreversible capacity of 126 mAh g^{-1}, which is calculated from the irreversible loss of oxygen together with lithium removal evolving O_2. Moreover, the rechargeable capacity observed at 55 ^oC is 300 mAh g^{-1}, which is larger than the expected value of 252 mAh g^{-1}. These results can hardly support the mechanism of irreversible loss of oxygen. So they speculated that the abnormal capacity is based on "cation" (Mn^{4+} / Mn^{5+}, Mn^{6+}) or "anion" (O^{2-} / O_2^{2-}) redox reaction. Koga *et al.*[27] combined the investigations of redox titration, magnetic measurement, neutron diffraction and chemical analyzes to deduce that lattice oxygen participate in the redox processes. Within the bulk oxygen is oxidized without oxygen loss in the initial charge and can be reduced in the subsequent discharge, whereas at surface oxygen is oxidized to O_2 and irreversibly lost from the structure. They also found that the manganese ions are mainly at the tetravalent state, only a few of them are reduced to trivalent state to compensate for the surface oxygen loss. Ito *et al.*[28] employed *in situ* X-ray absorption spectroscopy (XAS) to examine the changes of the valence states of Ni, Co and Mn in $Li[Ni_{0.17}Li_{0.2}Co_{0.07}Mn_{0.56}]O_2$, specifically focused on the Mn K preedge during charge-discharge, and obtained the same results. Sathiya *et al.*[29,30] further confirmed that the extra capacity of Li-rich layered oxides can be attributed to the reversible anionic ($O^{2-} \rightarrow O_2^{n-}$ where $3 > n > 1$) redox processes by complementary XPS and

electron paramagnetic resonance (EPR) experiments.

Although the above reports have provided enough evidences to support the existence of reversible anionic redox processes during charge-discharge, they are still insufficient to make a conclusion that the origin of the abnormal capacity of Li-rich layered oxides has been identified. Actually, the reversible redox processes of oxygen have also been reported in the conventional materials. Petersburg *et al.*[31] reported that oxygen and transition metal both involved in the charge compensation mechanism of $LiNi_{1/3}Mn_{1/3}Co_{1/3}O_2$ cathodes. While Ni is found to be the only transition metal involved in the charge compensation reaction until half the Li is removed, the second half of the deintercalation reaction is not accompanied by transition-metal oxidation. It is deduced that over the second half of Li deintercalation, the oxidation of oxygen ions bonded to cobalt is responsible for charge compensation. Kosova *et al.*[32] conducted X-ray, IRS, XPS, EDRS and magnetic measurements and confirmed that oxygen ions in $Li_{1+x}CoO_2$ ($0 < x \leq 0.1$) do compensate for the charge upon chemical delithiation. Mukerjee *et al.*[33,34] employed *in situ* XAS measurements to study Zn doped lithiated Mn spinel $LiZn_{0.5-x}Mn_{1.5+x}O_4$ ($0 \leq x \leq 0.5$) and suggested that O^{2-} ions in the Zn-spinel lattice are partially oxidized to O^- at the 5 V plateau during the anodic process and O^- ions are reduced back to O^{2-} during the cathodic process at the 5 V plateau. In view of the above results and with the consideration of the structure characteristics of Li-rich layered oxides, it is reasonable to deduce that the reversible redox processes of oxygen maybe take place in the layered $LiMO_2$ component rather than in Li_2MnO_3 component. To the best of our knowledge, the reaction process at 4.5

V plateau is so complex that the precision structure of the delithiated product after initial charge is still acataleptic. So the extra capacity may come from some other undiscovered reaction mechanisms rather than reversible redox processes of oxygen as previously reported. Therefore, in order to eliminate the uncertainty discussed above, some new work should be done.

In this paper, we designed a set of comparison experiments using XPS measurements to confirm whether Li_2MnO_3 component participates in the reversible redox processes of oxygen during initial charge-discharge. The Li-rich layered oxide we employed here was $Li_{1.14}Ni_{0.136}Co_{0.136}Mn_{0.544}O_2$. Since Li-rich layered oxides consist of rock salt Li_2MnO_3-like component and layered $LiMO_2$ component, we chose pure Li_2MnO_3 and $LiNi_{0.5}Co_{0.2}Mn_{0.3}O_2$ as comparisons. Besides, we also adopted the most common layered oxide $LiCoO_2$ as reference. Chemical delithiation and lithiation treatments were introduced to simulate the electrochemical charge-discharge processes.[35-38] The absence of unnecessary distractions like carbon, polyvinylidene fluoride (PVdF) and deposition resulting from electrolyte oxidation in the electrode makes the XPS analysis especially easier.

Experimental

Material preparation and treatment

Layered $Li_{1.14}Ni_{0.136}Co_{0.136}Mn_{0.544}O_2$ was synthesized by a co-precipitation method. The spherical $(Mn_{0.544}Ni_{0.136}Co_{0.136})CO_3$ precursors were first prepared with a desired stoichiometric ratio of Mn, Ni, Co sulphates and Na_2CO_3 aqueous solution. Then the obtained precursors were mixed with proper amounts of Li_2CO_3. Finally, the resultant

mixture was heated in air at 500 °C for 5 h followed by heating at 850 °C for 10 h. Li_2MnO_3 was prepared using a sol-gel method. In a typical process, 100 mL of an aqueous solution containing metal acetates with a molar ratio Li : Mn of 2.03 : 1 (concentration of metal ions was 1 M) was slowly dripped into 50 mL citric acid (same number of moles as the metal ions) aqueous solution with constant stirring. The solution PH was then adjusted to 7.5 using ammonium hydroxide, prior to solvent evaporation at 75 ^oC in a water bath until a brown gel was obtained. The gel was further dried at 120 ^oC for 24 h to form a fluffy precursor, followed by calcination at 450 ^oC for 5 h in air and thoroughly ground using a mortar and pestle. The obtained power was heated at 750 ^oC for 12 h in air at a heating rate of 5 $^oC\ min^{-1}$, and then furnace-cooled. Layered $LiNi_{0.5}Co_{0.2}Mn_{0.3}O_2$ and $LiCoO_2$ were bought form *Ningbo Veken Battery Co. Ltd*.

In order to avoid the structural collapses under high delithiated state, the amount of chemical extracted lithium compared to the corresponding material was designed as a molar ratio of 0.1 : 1. The as-prepared $Li_{1.14}Ni_{0.136}Co_{0.136}Mn_{0.544}O_2$, Li_2MnO_3, $LiCoO_2$ and $LiNi_{0.5}Co_{0.2}Mn_{0.3}O_2$ powders (3 g) were first dispersed into 100 ml anhydrous acetonitrile respectively. Then the right amounts of 0.5M NO_2BF_4 (Aladdin, AR) acetonitrile solutions were slowly dripped into the obtained suspensions and continuously stirred for 12 h to extract lithium. Chemical lithium reinsertion was accomplished by adding a 0.5 M LiI (Aladdin, AR) acetonitrile solution in excess into the delithiated material in acetonitrile. The mixture was maintained under stirring for 24 h. All the powders obtained after chemical delithiation and lithiation were washed

thoroughly with acetonitrile. All the experiments were carried out in an argon filled glove box.

Characterization

Li, Co, Ni and Mn contents included in the materials were determined using an inductively coupled plasma-atomic emission spectrometry (ICP, Optima 2100) after the powders completely dissolved into an acidic solution. The crystal structures were confirmed by X-ray diffractometer (D8 Advance, Bruker AXS) using Cu-Kα radiation source (λ1 = 1.54056 Å, λ2 = 1.54439 Å) with a scan rate of 7° min^{-1} between 10 and 80° 2θ. The Rietveld refinement of the XRD data was performed using the Jade 6.5 software. XPS measurements were carried out with an X-ray photoelectron spectrometer (Kratos AXIS Ultra DLD), using a focused monochromatized Al Kα radiation (1,486.6 eV). Curve fitting of slow-scanned XPS spectra was carried out using a peak-fit program with a Gaussian-Lorentzian sum function. The binding energy scale was calibrated from the hydrocarbon contamination using the C1s peak at 284.8 eV. TGA curves were recorded using a thermogravimetric/differemtial thermal analyser (Perkin-Elmer, Pyris Diamond TG/DTA) in air at a heating rate of 5 $^{o}C\ min^{-1}$ from room temperature to 600 ^{o}C.

Electrochemical measurement

The electrochemical cycling tests were conducted using CR2032-type coin cells with lithium metal as negative electrodes. Composite positive electrodes consisted of 80 wt.% active material, 10 wt.% Super P, and 10 wt.% PVdF binder in

N-methyl-2-pyrrolidone (NMP), pasted on an aluminium foil as a current collector. They were then pressed at 8 MPa after drying at 80 °C overnight. A 1M $LiPF_6$ solution in a mixture of ethylene carbonate (EC) and dimethylcarbonate (DMC) in a 3:7 ratio by volume was employed as electrolyte (Guotai-Huarong New Chemical Material Co.,Ltd). The cells were assembled in an argon filled glove box. The galvanostatic charge-discharge tests were carried out at room temperature using a LAND battery program-control test system (Wuhan, China). All the cells were cycled between 2.0 and 4.6 V versus Li^+ / Li at 0.1 C.

Results and discussion

NO_2BF_4 was chosen as the oxidant to extract lithium ions and LiI was chosen as the reductant to reinsert lithium ions. Since the redox couple NO_2^+/NO_2 is reported to correspond to an oxidizing voltage of 5.1 V vs. Li^+/Li,[38] which is well above the end-of-charge voltages of $Li_{1.14}Ni_{0.136}Co_{0.136}Mn_{0.544}O_2$ (4.6 V), Li_2MnO_3 (4.6 V), $LiCoO_2$ (4.2 V) and $LiNi_{0.5}Co_{0.2}Mn_{0.3}O_2$ (4.3 V), it is reasonable to deduce that lithium can be easily extracted from these materials. LiI is reported as a mild reducing agent with a voltage for I^-/I^0 redox couple close to 3 V vs. Li^+/Li,[39] so the materials previously delithiated should be lithiated after soaking in LiI acetonitrile solution for enough time.

Table 1 shows the contents of lithium, nickel, cobalt, manganese metal ions in the materials determined by ICP (fixing the total amount of transition metal ions as constant in each material) before and after chemical delithiation and lithiation. The stoichiometric ratio of the elements in each pristine material is very close to the

chemical formula as expected. No significant difference in the relative contents of transition metal ions was observed. After chemical delithiation, about 0.1 mol Li^+ ions were extracted from each material (0.07 mol for $Li_{1.14}Ni_{0.136}Co_{0.136}Mn_{0.544}O_2$, 0.12 mol for Li_2MnO_3, 0.14 mol for $LiCoO_2$ and 0.04 mol for $LiNi_{0.5}Co_{0.2}Mn_{0.3}O_2$, the different amount of extracted lithium may depend on the nature of the materials and some experimental errors), which is basically consistent with the dosage of NO_2BF_4. The chemical analyses also show that the delithiated materials could be successfully lithiated by LiI in excess and the final compositions in metal ions were similar to the pristine materials.

Fig. 1 gives a comparison of the XRD patterns obtained for the materials before and after chemical delithiation and lithiation. In Fig. 1(a), all the samples can be indexed in a well-defined trigonal α-$NaFeO_2$ or rhombohedral α-$NaFeO_2$ layered structure with a space group *R-3m* except the extra peaks around 20 to 25° *2θ* due to $LiMn_6$ super lattice reflections in the transition metal layers, which have been identified with the monoclinic Li_2MnO_3 component (space group: *C2/m*).[5,18,20] In Fig. 1(b), the large full width at half maximum (FWHM) of spectral lines imply that the Li_2MnO_3 particles prepared by a sol-gel method have a small size. In Fig. 1(c) and (d), the patterns of $LiCoO_2$ and $LiNi_{0.5}Co_{0.2}Mn_{0.3}O_2$ are similar and can be indexed in α-$NaFeO_2$-type unit cells described in the space group *R-3m*. For all the materials, no obvious change can be observed among the patterns, suggesting that their structures remain stable during chemical delithiation and lithiation. The cell parameters determined from the Rietveld Refinement of the XRD data are given in Table 2. For

$Li_{1.14}Ni_{0.136}Co_{0.136}Mn_{0.544}O_2$, both the *a* axis and the cell volume decrease after chemical delithiation and increase after chemical lithiation while the *c* axis increases after chemical delithiation and increases again after chemical lithiation. The above change processes are consistent with the previous reported results during electrochemical cycle.[19] $LiCoO_2$ and $LiNi_{0.5}Co_{0.2}Mn_{0.3}O_2$ go through the same processes with $Li_{1.14}Ni_{0.136}Co_{0.136}Mn_{0.544}O_2$ except Li_2MnO_3. The cell volume of Li_2MnO_3 does not increase but reduce after chemical lithiation, indicating that its lattice structure has changed. But the amount of structural transformation is so small that the XRD pattern cannot obviously display the difference. Detailed discussion about this phenomenon will be provided in the XPS analysis section below.

In order to detect the influence of chemical delithiation and lithiation on electrochemical performance, electrochemical tests were also performed. The initial charge-discharge curves of all the materials are shown in Fig. 2. After the chemical delithiation, serious electrode polarization phenomena were observed in the charge-discharge curves of $Li_{1.14}Ni_{0.136}Co_{0.136}Mn_{0.544}O_2$, $LiCoO_2$ and $LiNi_{0.5}Co_{0.2}Mn_{0.3}O_2$. They can be attributed to the lattice distortions formed during the oxidation process, which increase the impedances of the batteries. For $Li_{1.14}Ni_{0.136}Co_{0.136}Mn_{0.544}O_2$ (chemical delithiated) shown in Fig 2(a), the plateau around 4.5 V disappears and the discharge capacity decays to 114 mAh g^{-1}, which is much smaller than the pristine material of 245 mAh g^{-1}. Interestingly, the electrode polarization phenomenon subsides after chemical lithiation. The plateau around 4.5 V appears again and the discharge capacity increases to 246 mAh g^{-1}, just as the pristine

material. However, there is an obvious difference, a voltage plateau at about 3 V, in the discharge curve. The differential discharge capacity (dQ/dV) plots illustrated in Fig. S1 further confirm that a reduction peak at about 3 V appears after chemical lithiation. This might be induced by the phase separation between the chemical activated region at the particle surface and the raw region in the bulk. Fig. 2(b) shows that the chemical delithiation does not lead to capacity attenuation for Li_2MnO_3. On the contrary, the discharge capacity increases due to the first cycle coulombic efficiency exceeding 100%. We believe that the lithium vacancies formed during chemical delithiation are retained and can insert lithium ions again during electrochemical discharge. In Fig. 2(c) and (d), the initial charge-discharge capacities of $LiCoO_2$ and $LiNi_{0.5}Co_{0.2}Mn_{0.3}O_2$ recovered after the chemical delithiation are much lower than the pristine materials, which is consistent with result of $Li_{1.14}Ni_{0.136}Co_{0.136}Mn_{0.544}O_2$. However, the initial charge-discharge capacities of $LiCoO_2$ and $LiNi_{0.5}Co_{0.2}Mn_{0.3}O_2$ recovered after the chemical delithiation and lithiation do not increase to the levels of the pristine materials. Since the potential imposed by the redox couple NO_2^+/NO_2 (5.1 V vs. Li^+/Li) is much higher than the normal end-of-charge voltages of $LiCoO_2$ (4.2 V) and $LiNi_{0.5}Co_{0.2}Mn_{0.3}O_2$ (4.3 V), it is reasonable to deduce that the reactions to extract lithium ions are so violent that the distorted lattice cannot recover easily. Actually, their capacities will experience a slowly increasing process in the following electrochemical cycles, as shown in Fig. 3. In addition, it is necessary to point out that the spikes appeared at the beginning of the initial charge curves are closely related to the large amount of Li_2CO_3 formed at the

particle surface, which need to be decomposed first before the lithium ions in cathode materials can be extracted.

From the above results, it is clear that chemical delithiation and lithiation with NO_2BF_4 and LiI is a very effective method to simulate the process of electrochemical charge-discharge, in good agreement with the results already reported by Koga at al.[27] Therefore, the following of this paper will focus on the characterization of the oxidation state of lattice oxygen, in order to confirm whether the oxygen ions participated in the charge and discharge reactions come from the Li_2MnO_3 component or not.

XPS measurements were performed to compare the pristine materials and the materials recovered after chemical delithiation and lithiation. The obtained O 1s spectra were shown in Fig. 4. Three representative deconvoluted peaks were observed in all the samples as expected. One of which corresponds to lattice oxygen with a binding energy of 529.4 eV for Li_2MnO_3 or 529.5 eV for $Li_{1.14}Ni_{0.136}Co_{0.136}Mn_{0.544}O_2$, $LiCoO_2$ and $LiNi_{0.5}Co_{0.2}Mn_{0.3}O_2$.[40,41] The others are associated with the adsorbed surface species, which depend strongly upon the history of the sample. For $Li_{1.14}Ni_{0.136}Co_{0.136}Mn_{0.544}O_2$ and $LiCoO_2$, the O 1s peak at 531.2 eV contains contributions from surface CO_3^{2-} and -OH, the common impurities at the surface of air exposed $LiMO_2$ (M = Ni, Co, Mn and so on) materials, resulting from the adsorption of CO_2 and water from the ambient either upon storage or during synthesis process.[42,43] For Li_2MnO_3 and $LiNi_{0.5}Co_{0.2}Mn_{0.3}O_2$, the O 1s peak at 531.5 eV indicates the existence of Li_2CO_3 on the surface of the materials.[41] The remaining

feature at ~533.8 eV can be attributed to the oxygen bound to the alkyl group in organic or semiorganic carbonates.[44] In Fig. 4(a), a new component at ~530.5 eV appears after chemical delithiation. It corresponds to oxide ions with a lower electronic density as compared with O^{2-} ions and can be identified as the existence of formed O_2^{2-} species or under-coordinated oxygen atoms. Moreover, it disappears after chemical lithiation and the shape of the O 1s spectrum converts back to the pristine. The above phenomena demonstrate the redox activity of lattice oxygen in Li-rich layered oxides and are well consistent with the results previously reported by M. Sathiya et al.[29,30] It is important to note that similar phenomena are also observed in Li_2MnO_3, as shown in Fig. 4(b). The same O 1s peak with a binding energy at 530.5 eV appears after chemical delithiation and disappears after chemical lithiation, indicating that part of lattice oxygen experience a redox process to compensate for the charge upon chemical delithiation and lithiation. The new peak with a binding energy at 530.1 eV formed after chemical lithiation confirms the existence of O^{2-} in $LiMn_2O_4$ environment.[45,46] Pure Li_2MnO_3 is reported as quite unstable when cycled above the activation voltage platform of 4.5 V and tends to transform into $LiMn_2O_4$.[47] Combined with the reduced cell volume discussed above, it is reasonable to deduce that the structural transformation from Li_2MnO_3 to $LiMn_2O_4$ occurs in chemical delithiation and lithiation. Fig. 4(c) shows that the O 1s spectra of $LiCoO_2$ do not change, in addition to the enhanced intensity of Li_2CO_3. Therefore, it can be certain that lattice oxygen in $LiCoO_2$ do not participate in the charge compensation, at least, not under this low delithiated degree. The formation of Li_2CO_3 at particle surface can

be attributed to the existence of unstable Co^{n+} ($2 < n \leq 4$), which can absorb CO_2 in air during storage. This phenomenon is more obvious for Ni-rich cathode materials,[48-51] as shown in Fig. 4(d). The strong peak at 531.5 eV indicates a large amount of Li_2CO_3 existed at the surface of the pristine $LiNi_{0.5}Co_{0.2}Mn_{0.3}O_2$. Since the lithium ions are extracted from the material in a form of Li_2O during the formation of Li_2CO_3, a NiO-like crystal structure is always observed in the nearsurface regions. The new peak at 530.7 eV appeared after chemical delithiation corresponds to the defect oxygen species in partly oxidized NiO-like region, where Ni^{3+} is reported as a "defect structure" and the O 1s is generally at values well in excess of 530 eV.[52-55] It does not vanish after chemical lithiation, indicating that the partly oxidized NiO-like is stable with LiI. In a word, the above results demonstrate that part of lattice oxygen in $Li_{1.14}Ni_{0.136}Co_{0.136}Mn_{0.544}O_2$ and Li_2MnO_3 participate in the charge compensation upon chemical delithiation and lithiation, while in $LiCoO_2$ and $LiNi_{0.5}Co_{0.2}Mn_{0.3}O_2$ does not, which means that the extra capacity of Li-rich layered oxides comes from the reversible redox process of oxygen in Li_2MnO_3 component.

On consideration of the poor thermal stability of the formed O_2^{2-} spieces, TGA was employed to further demonstrate the conclusions we made above. Fig. 5(a) shows the TG curves of the pristine materials. Their weights decrease gradually with the increase of temperature. It is certain that the quality loss mainly come from the evaporation of the absorbed species, and the release of some lattice oxygen under high temperature, especially for Li_2MnO_3. For the materials recovered after chemical delithiation, as shown in Fig. 5(b), a sudden quality loss in

$Li_{1.14}Ni_{0.136}Co_{0.136}Mn_{0.544}O_2$ at about 210 ^oC is very conspicuous. Since the evaporation of the absorbed species is a slow process, the only explanation for this phenomenon is that the formed O_2^{2-} species decomposes ($O_2^{2-} \rightarrow O^{2-} + 1/2\ O_2$) at this temperature and the resultant O_2 releases from the material surface. Fig. S2 examines the XRD pattern of the sample recovered after chemical delithiation and annealing at 300 ^oC. However, there is no visible difference can be found when compared with the pristine sample or the sample recovered after chemical delithiation. It means that the amount of phase change after the decomposition of O_2^{2-} is so small that the XRD technique is failed to detect accurately. In Fig. S3, the O1s XPS spectra show that the peak of O_2^{2-} species disappears after annealing at 300 ^oC for the sample recovered after chemical delithiation, which confirms the decomposition of O_2^{2-}. All the results above are consistent with the results reported in our previous paper,[3] which detailed studied the process of phase transformation from layered to spinel for the chemical delithiated material during heat treatment. Therefore, we are sure that the surface structure of the chemical delithiated sample here will transform from layered to spinel after the decomposition of O_2^{2-} at about 210 ^oC. Similar phenomenon is also observed in Li_2MnO_3, which starts to lose weight quickly at about 150 ^oC due to its unstable structure. $LiCoO_2$ and $LiNi_{0.5}Co_{0.2}Mn_{0.3}O_2$ are relatively stable during the heating process. The quality loss of $LiNi_{0.5}Co_{0.2}Mn_{0.3}O_2$ starts at about 400 ^oC. It can be attributed to the decomposition of the delithiated section, resulting in a rock-salt NiO-type structure, which has been reported by Nam et al.[56] Fig. 5(c) shows that the structures of the chemical lithiated materials become stabilized because the amounts

of the quality loss decrease obviously. Although $Li_{1.14}Ni_{0.136}Co_{0.136}Mn_{0.544}O_2$ recovered after chemical delithiation and lithiation is still less stable than the pristine one, it does not experience a sudden quality loss at about 210 ^oC. Therefore, it is reasonable to deduce that the formed O_2^{2-} species has been reduced after chemical lithiation. The above results are well consistent with the results obtained in XPS analysis section, so a conclusion can be made that lattice oxygen in the Li_2MnO_3 component participate in the charge compensation during charge-discharge for Li-rich layered oxides.

Besides, the results also educe a conclusion that there is a contradiction between high capacity and good thermal stability. Li-rich layered oxides are attractive for their high capacities, but the high capacities are based on the activation of the Li_2MnO_3 component, which will form the O_2^{2-} species, resulting in the degradation of thermal stability. It is foreseeable that the fully delithiated Li-rich layered oxides (here x = 0.1 as designed) will generate more O_2 at about 210 ^oC. And such a large amount of O_2 suddenly releases from the cathode electrode will be very dangerous for a sealed single battery, not to mention a stack in practical application. Since safety is an indispensable criterion, the available capacity for Li-rich layered oxides will be restricted.

Conclusions

This study successfully employs chemical delithiation (NO_2BF_4) and lithiation (LiI) to simulate electrochemical charge and discharge. Through the comparisons of the O 1s spectra obtained from XPS measurements, it is confirmed that the reversible redox

processes of oxygen reported in Li-rich layered oxides occur in the Li_2MnO_3 component. Therefore, the charge compensation from lattice oxygen is responsible for the extra capacity of Li-rich layered oxides. For future, more work should be focused on the exploration of the precision structure in the delithiated material. It will be a key to discover a vast number of high-capacity cathode materials.

In addition, the poor thermal stability of these materials could be an intrinsic defect which is almost impossible to overcome due to the decomposition of O_2^{2-} under high temperature (210 ^oC). It is surely that this finding will be a big challenge for these materials' practical application.

Acknowledgements

This work was financially supported by the Key Research Program of the Chinese Academy of Science (KGZD-EW-202-4), the Science and Technology Service Network Initiative of the Chinese Academy of Science (KFJ-EW-STS-110), the Ningbo Science and Technology Innovation Team (2012B82001) and the National Natural Science Foundation of China (21403263).

References

[1] M. Armand and J. M. Tarascon, *Nature*, 2008, **451**, 652.

[2] J. Zheng, M. Gu, J. Xiao, B. J. Polzin, P. Yan, X. Chen, C. Wang and J.-G. Zhang, *Chem. Mater.*, 2014, **26**, 6320.

[3] S. J. Han, B. Qiu, Z. Wei, Y. G. Xia and Z. P. Liu, *J. Power Sources*, 2014, **268**, 683.

[4] H. J. Yu and H. S. Zhou, *J. Mater. Chem.*, 2012, **22**, 15507.

[5] M. M. Thackeray, S. H. Kang, C. S. Johnson, J. T. Vaughey, R. Benedek and S. A. Hackney, *J. Mater. Chem.*, 2007, **17**, 3112.

[6] J. Wang, G. X. Yuan, M. H. Zhang, B. Qiu, Y. G. Xia and Z. P. Liu, *Electrochim. Acta*, 2012, **66**, 61.

[7] M. Gu, I. Belharouak, A. Genc, Z. Wang, D. Wang, K. Amine, F. Gao, G. Zhou, S. Thevuthasan, D. R. Baer, J.-G. Zhang, N. D. Browning, J. Liu and C. Wang, *Nano Lett.*, 2012, **12**, 5186.

[8] J. Cho, Y. J. Kim and B. Park, *Chem. Mater.*, 2000, **12**, 3788.

[9] J. M. Tarascon, E. Wang, F. K. Shokoohi, W. R. McKinnon and S. Colson, *J. Electrochem. Soc.*, 1991, **138**, 2859.

[10] A. Yamada, S. C. Chung and K. Hinokuma, *J. Electrochem. Soc.*, 2001, **148**, A224.

[11] K. A. Jarvis, Z. Q. Deng, L. F. Allard, A. Manthiram and P. J. Ferreira, *Chem. Mater.*, 2011, **23**, 3614.

[12] H. Koga, L. Croguennec, P. Mannessiez, M. Ménétrier, F. Weill, L. Bourgeois, M. Duttine, E. Suard and C. Delmas, *J. Phys. Chem. C*, 2012, **116**, 13497.

[13] T. Ohzuku, M. Nagayama, K. Tsujia and K. Ariyoshia, *J. Mater. Chem.*, 2011, **21,** 10179.

[14] D. Wang, I. Belharouak, X. Zhang, Y. Ren, G. Meng and C. Wang, *J. Electrochem. Soc.*, 2014, **161**, A1.

[15] C. S. Johnson, J-S. Kim, C. Lefief, N. Li, J. T. Vaughey and M. M. Thackeray, *Electrochem. Commun.*, 2004, **6**, 1085.

[16] M. M. Thackeray, C. S. Johnson, J. T. Vaughey, N. Li and S. A. Hackney, *J. Mater. Chem.*, 2005, **15**, 2257.

[17] H. J. Yu, R. Ishikawa, Y.-G. So, N. Shibata, T. Kudo, H. S. Zhou and Y. Ikuhara, *Angew. Chem. Int. Ed.*, 2013, **52**, 5969.

[18] Z. H. Lu, D. D. MacNeil and J. R. Dahna, *Electrochem. Solid-State Lett.*, 2001, **4**, A191.

[19] Z. H. Lua and J. R. Dahna, *J. Electrochem. Soc.*, 2002, **149**, A815.

[20] M. Gu, A. Genc, I. Belharouak, D. Wang, K. Amine, S. Thevuthasan, D. R. Baer, J.-G. Zhang, N. D. Browning, J. Liu and C. Wang, *Chem. Mater.*, 2013, **25**, 2319.

[21] A. R. Armstrong, M. Holzapfel, P. Novák, C. S. Johnson, S.-H. Kang, M. M. Thackeray and P. G. Bruce, *J. Am. Chem. Soc.*, 2006, **128**, 8694.

[22] Y.-S. Hong, Y. J. Park, K. S. Ryu, S. H. Change and M. G. Kim, *J. Mater. Chem.*, 2004, **14**, 1424.

[23] J. Zheng, W. Shi, M. Gu, J. Xiao, P. Zuo, C. Wang and J.-G. Zhang, *J. Electrochem. Soc.*, 2013, **160**, A2212.

[24] J. Zheng, M. Gu, J. Xiao, P. Zuo, C. Wang and J.-G. Zhang, *Nano Lett.*, 2013, **13**, 3824.

[25] J. Zheng, M. Gu, A. Genc, J. Xiao, P. Xu, X. Chen, Z. Zhu, W. Zhao, L. Pullan, C. Wang and J.-G. Zhang, *Nano Lett.*, 2014, **14**, 2628.

[26] T. Ohzuku, M. Nagayama, K. Tsuji and K. Ariyoshi, *J. Mater. Chem.*, 2011, **21**, 10179.

[27] H. Koga, L. Croguennec, M. Ménétrier, K. Douhil, S. Belin, L. Bourgeois, E.

Suard, F. Weill and C. Delmas, *J. Electrochem. Soc.*, 2013, **160**, A786.

[28] A. Ito, Y. Sato, T. Sanada, M. Hatano, H. Horie and Y. Ohsawa, *J. Power Sources*, 2011, **196**, 6828.

[29] M. Sathiya, K. Ramesha, G. Rousse, D. Foix, D. Gonbeau, A. S. Prakash, M. L. Doublet, K. Hemalatha and J.-M. Tarascon, *Chem. Mater.*, 2013, **25**, 1121.

[30] M. Sathiya, G. Rousse, K. Ramesha, C. P. Laisa, H. Vezin, M.-L. Doublet, D. Foix, D. Gonbeau, W. Walker, A. S. Prakash, M. Ben Hassine, L. Dupont and J.-M. Tarascon, *Nat. Mater.*, 2013, **12**, 827.

[31] C. F. Petersburg, Z. Li, N. A. Chernova, M. S. Whittingham and F. M. Alamgir, *J. Mater. Chem.*, 2012, **22**, 19993.

[32] N. V. Kosova, V. V. Kaichev, V. I. Bukhtiyarov, D. G. Kellerman, E. T. Devyatkina and T. V. Larina, *J. Power Sources*, 2003, **119-121**, 669.

[33] S. Mukerjeea, X. Q. Yang, X. Sun, S. J. Lee, J. McBreen and Y. Ein-Eli, *Electrochim. Acta.*, 2004, **49**, 3373.

[34] W. Wen, B. Kumarasamy, S. Mukerjee, M. Auinat and Y. Ein-Eli, *J. Electrochem. Soc.*, 2005, **152**, A1902.

[35] S. Kikkawa, S. Miyazaki and M. Koizumi, *J. Solid State Chem.*, 1986, **62**, 35.

[36] R. Gupta and A. Manthiram, *J. Solid State Chem.*, 1996, **121**, 483.

[37] X.-J. Wang, H.-Y. Chen, X. Q. Yu, L. J. Wu, K.-W. Nam, J. M. Bai, H. Li, X. J. Huang and X.-Q. Yang, *Chem. Commun.*, 2011, **47**, 7170.

[38] A .R. Wizansky, P. E. Rauch and F. J. Disalvo, *J. Solid State Chem.*, 1989, **81**, 203.

[39] J. M. Tarascon and D. Guyomard, *J. Electrochem. Soc.*, 1991, **138**, 2864.

[40] J.-Z. Kong, H.-F Zhai, C. Ren, G.-A. Tai, X.-Y. Yang, F. Zhou, H. Li, J.-X. Li and Z. Tang, *J. Solid State Electrochem.*, 2014, **18**, 181.

[41] A. M. Andersson, D. P. Abraham, R. Haasch, S. MacLaren, J. Liu and K. Amine, *J. Electrochem. Soc.*, 2002, **149**, A1358.

[42] J. G. Li, L. Wang, Q. Zhang and X. M. He, *J. Power Sources*, 2009, **189**, 28.

[43] A. W. Moses, H. G. Garcia Flores, J.-G. Kim and M. A. Langell, *Appl. Surf. Sci.*, 2007, **253**, 4782.

[44] G. Zhuang, Y. Chen and N. P. J. Ross, *Langmuir*, 1999, **15**, 1470.

[45] C. V. Ramana, M. Massot and C. M. Julien, *Surf. Interface Anal.*, 2005, **37**, 412.

[46] S. Chitra, P. Kalyani, T. Mohan, R. Gangadharan, B. Yebka, S. Castro-Garcia, M. Massot, C. Julien and M. Eddrief, *J. Electroceram.*, 1999, **3:4**, 433.

[47] S. F. Amalraja, L. Burlakaa, C. M. Julienb, A. Maugerc, D. Kovachevad, M. Taliankere, B. Markovskya and D. Aurbacha, *Electrochim. Acta*, 2014, **123**, 395.

[48] K. Matsumoto, R. Kuzuo, K. Takeya and A. Yamanaka, *J. Power Sources*, 1999, **558**, 81.

[49] R. Moshtev, P. Zlatilova, S. Vasilev, I. Bakolova and A. Kozawa, *J. Power Sources*, 1999, **434**, 81.

[50] H. S. Liu, Z. R. Zhang, Z. L. Gong and Y. Yang, *Electrochem. Solid-State Lett.*, 2004, **7**, A190.

[51] K. Shizuka, C. Kiyohara, K. Shima and Y. Takeda, *J. Power Sources*, 2007, **166**, 233.

[52] L. Tan and W. C. Crone, *Acta Mater.*, 2002, **50**, 4449.

[53] J.-K. Kang and S.-W. Rhee, *Thin Solid Films*, 2001, **391**, 57.

[54] A. Davidson, J. F. Tempere, M. Che, H. Roulet and G. Dufour, *J. Phys. Chem.*, 1996, **100**, 4919.

[55] A. F. Carley, S. D. Jackson, J. N. O'Shea and M. W. Roberts, *Surf. Sci.*, 1999, **440**, L868.

[56] K.-W. Nam, S.-M. Bak, E. Hu, X. Yu, Y. Zhou, X, Wang, L. Wu, Y. Zhu, K.-Y. Chung and X.-Q. Yang, *Adv. Funct. Mater.*, 2013, **23**, 1047.

Table 1 Chemical compositions determined by ICP for $Li_{1.14}Ni_{0.136}Co_{0.136}Mn_{0.544}O_2$, Li_2MnO_3, $LiCoO_2$ and $LiNi_{0.5}Co_{0.2}Mn_{0.3}O_2$ before and after chemical delithiation and lithiation.

Sample	State	Li	Ni	Co	Mn
$Li_{1.14}Ni_{0.136}Co_{0.136}Mn_{0.544}O_2$	Pristine	1.19	0.130	0.135	0.551
	Delithiation	1.12	0.129	0.134	0. 553
	Lithiation	1.20	0.129	0.136	0.551
Li_2MnO_3	Pristine	2.05			1.00
	Delithiation	1.93			1.00
	Lithiation	2.03			1.00
$LiCoO_2$	Pristine	1.04		1.00	
	Delithiation	0.90		1.00	
	Lithiation	1.00		1.00	
$LiNi_{0.5}Co_{0.2}Mn_{0.3}O_2$	Pristine	1.04	0.512	0.188	0.300
	Delithiation	1.00	0.511	0189	0.300
	Lithiation	1.05	0.512	0.188	0.300

Table 2 Structural parameters of $Li_{1.14}Ni_{0.136}Co_{0.136}Mn_{0.544}O_2$, Li_2MnO_3, $LiCoO_2$ and $LiNi_{0.5}Co_{0.2}Mn_{0.3}O_2$ deduced from Rietveld Refinement of XRD data.

Sample	State	a(Å)	b(Å)	c(Å)	β angle(deg)	c/a	V(Å^3)
	Pristine	2.8503(2)		14.238(1)		4.995	100.18(2)
$Li_{1.14}Ni_{0.136}Co_{0.136}Mn_{0.544}O_2$	Delithiation	2.8491(2)		14.247(2)		5.001	100.15(3)
	Lithiation	2.8519(5)		14.250(2)		4.997	100.37(5)
	Pristine	4.9282(8)	8.5241(6)	5.0143(5)	109.20(1)		198.93(5)
Li_2MnO_3	Delithiation	4.9247(7)	8.5274(8)	5.0128(7)	109.13(1)		198.89(6)
	Lithiation	4.925(1)	8.5264(7)	5.0111(9)	109.10(1)		198.86(6)
	Pristine	2.8151(1)		14.046(1)		4.990	93.39(2)
$LiCoO_2$	Delithiation	2.8140(3)		14.046(2)		4.991	93.32(4)
	Lithiation	2.8153(1)		14.050(1)		4.991	93.44(1)
	Pristine	2.8683(4)		14.226(2)		4.960	101.36(4)
$LiNi_{0.5}Co_{0.2}Mn_{0.3}O_2$	Delithiation	2.8652(5)		14.248(3)		4.973	101.29(6)
	Lithiation	2.8697(1)		14.241(1)		4.963	101.57(1)

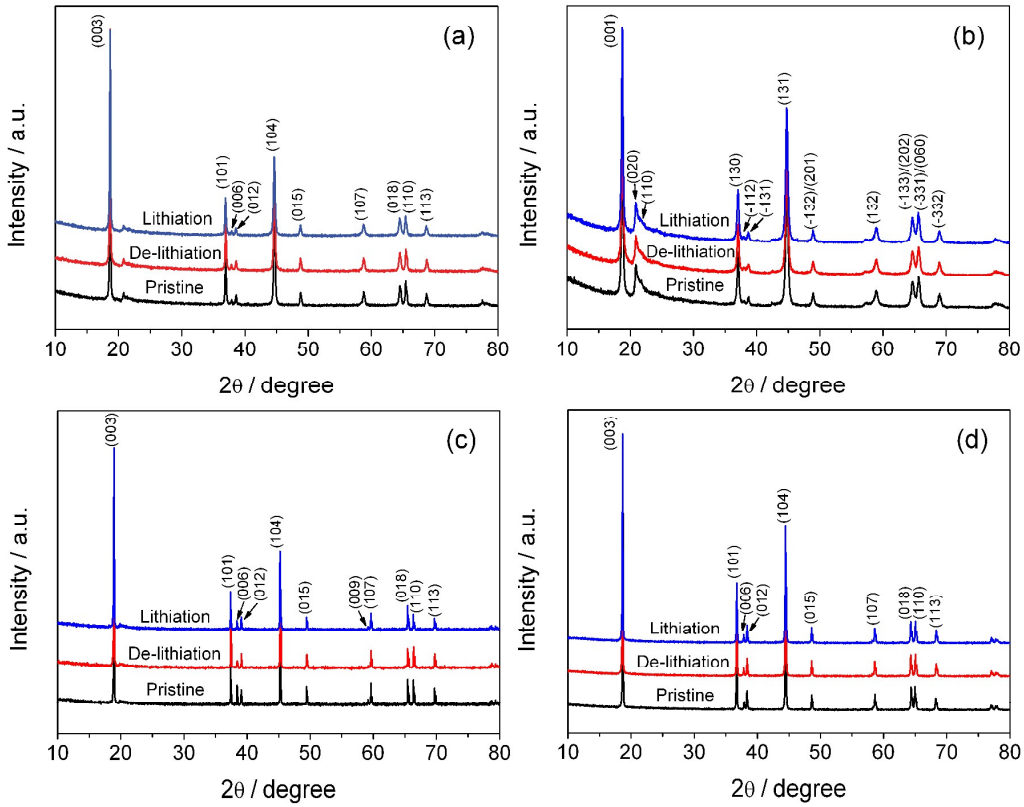

Fig. 1 XRD patterns of (a) $Li_{1.14}Ni_{0.136}Co_{0.136}Mn_{0.544}O_2$, (b) Li_2MnO_3, (c) $LiCoO_2$ and (d) $LiNi_{0.5}Co_{0.2}Mn_{0.3}O_2$. From bottom to top are the pristine sample, the delithiated sample and the lithiated sample in each pattern.

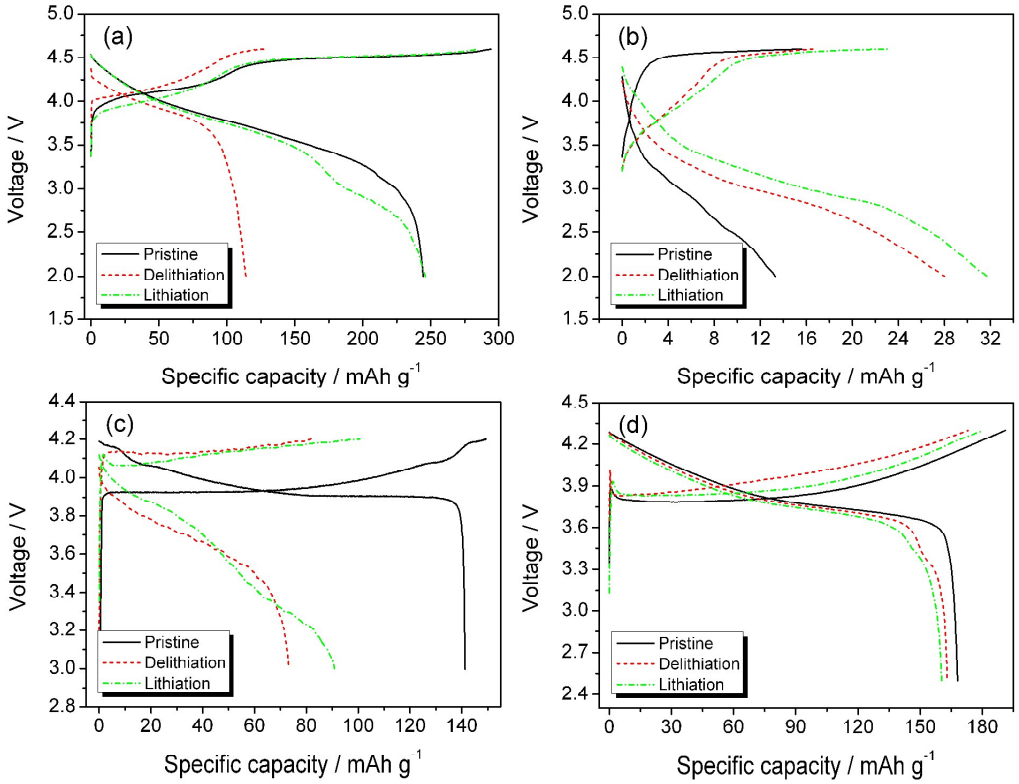

Fig. 2 Initial charge/discharge profiles of (a) $Li_{1.14}Ni_{0.136}Co_{0.136}Mn_{0.544}O_2$ (between 2.0 and 4.6 V at 0.1 C where 1 C = 250 mAh g^{-1}), (b) Li_2MnO_3 (between 2.0 and 4.6 V at 0.1 C where 1 C = 250 mAh g^{-1}), (c) $LiCoO_2$ (between 3.0 and 4.2 V at 0.1 C where 1 C = 140 mAh g^{-1}) and (d) $LiNi_{0.5}Co_{0.2}Mn_{0.3}O_2$ (between 2.5 and 4.3 V at 0.1 C where 1 C = 170 mAh g^{-1}). All the cells were tested at room temperature.

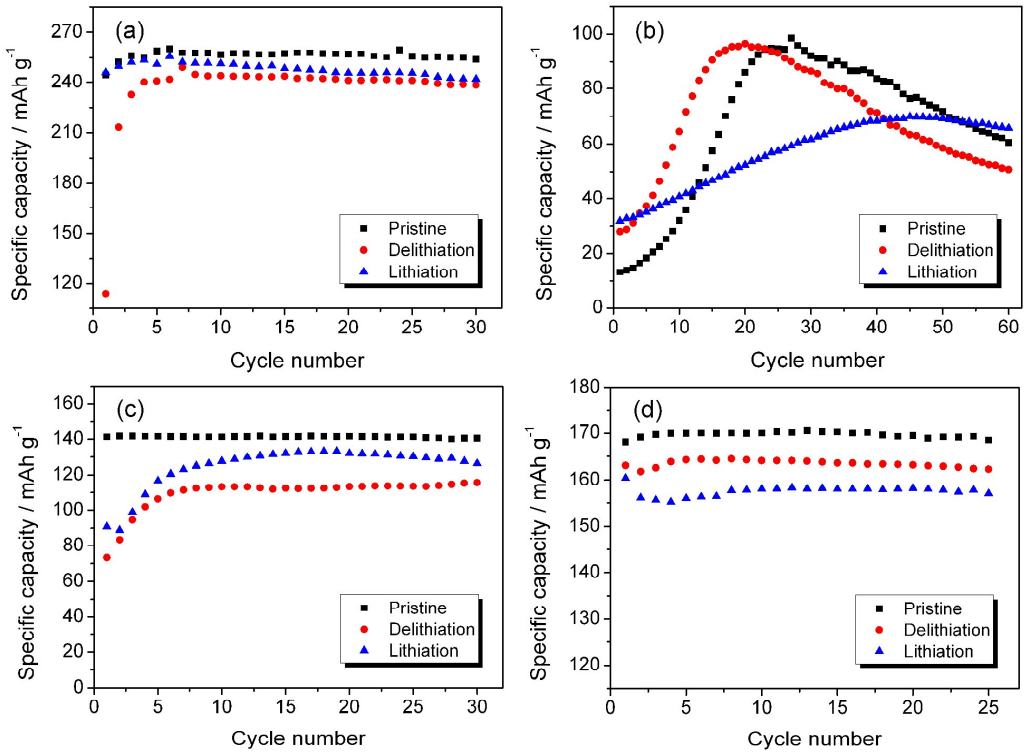

Fig. 3 Cycle performance of (a) $Li_{1.14}Ni_{0.136}Co_{0.136}Mn_{0.544}O_2$ (between 2.0 and 4.6 V at 0.1 C where 1 C = 250 mAh g^{-1}), (b) Li_2MnO_3 (between 2.0 and 4.6 V at 0.1 C where 1 C = 250 mAh g^{-1}), (c) $LiCoO_2$ (between 3.0 and 4.2 V at 0.1 C where 1 C = 140 mAh g^{-1}) and (d) $LiNi_{0.5}Co_{0.2}Mn_{0.3}O_2$ (between 2.5 and 4.3 V at 0.1 C where 1 C = 170 mAh g^{-1}). All the cells were cycled at room temperature.

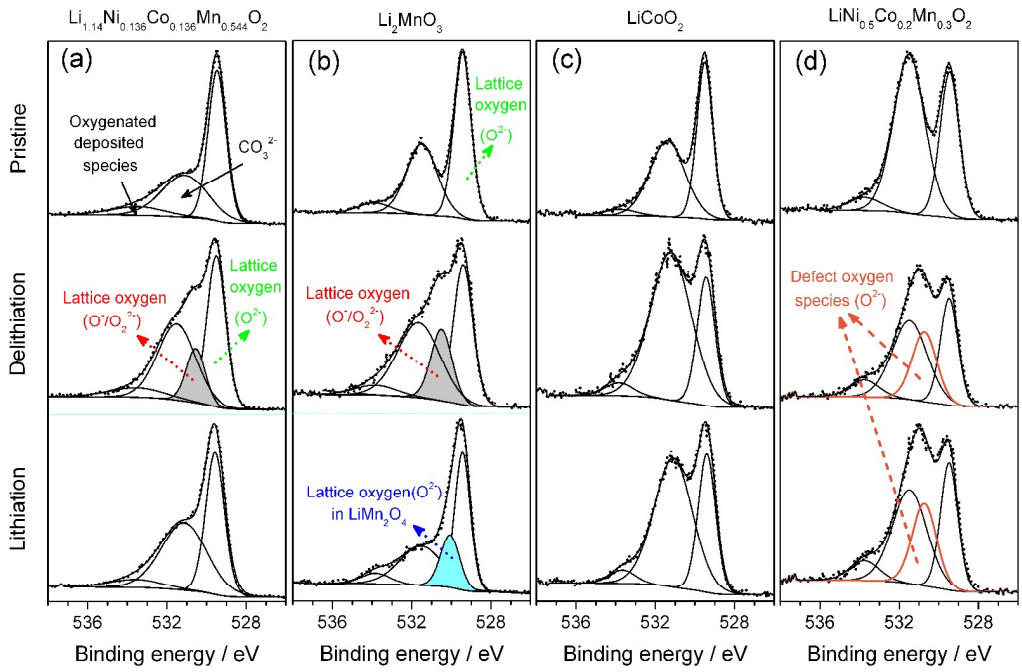

Fig. 4 XPS spectra of (a) $Li_{1.14}Ni_{0.136}Co_{0.136}Mn_{0.544}O_2$, (b) Li_2MnO_3, (c) $LiCoO_2$ and (d) $LiNi_{0.5}Co_{0.2}Mn_{0.3}O_2$. From top to bottom are the pristine sample, the de-lithiated sample and the lithiated sample in each spectrum. The short dot stands for the original data and the solid stands for the fitting data.

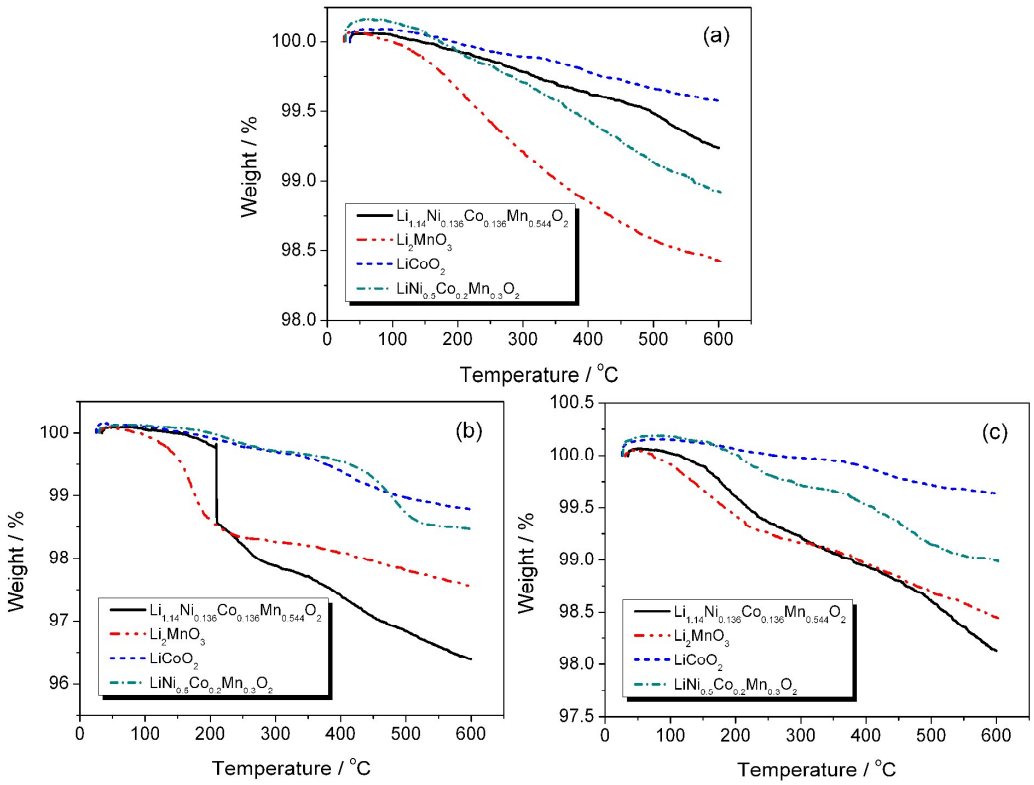

Fig. 5 TGA curves of (a) the pristine samples, (b) the chemical delithiated samples and (c) the chemical lithiated samples.

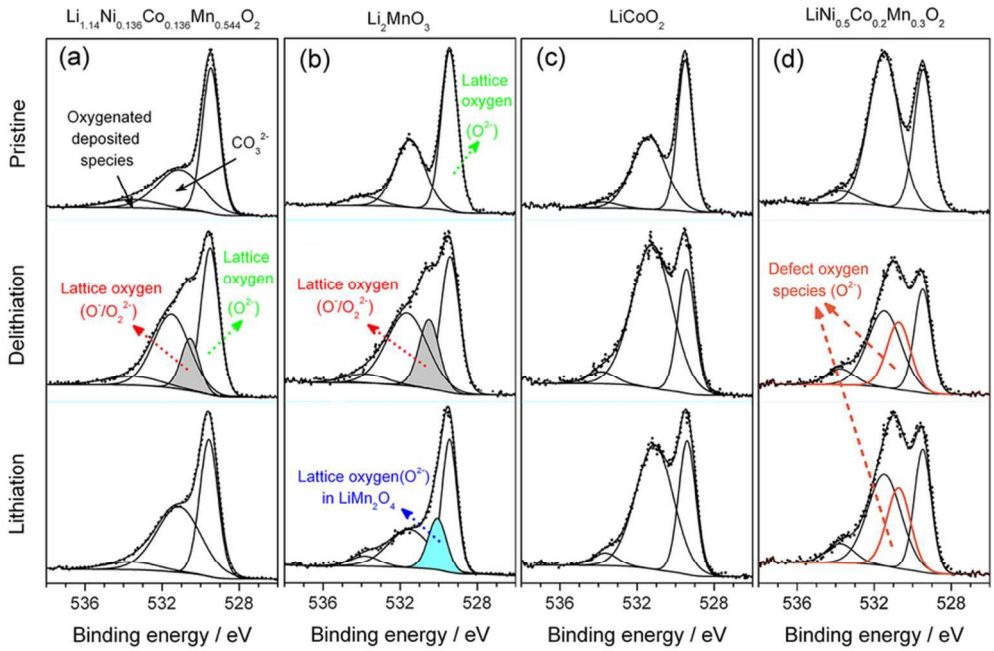

40x26mm (600 x 600 DPI)

The charge compensation from lattice oxygen in the Li_2MnO_3 component is responsible for the high specific capacity of Li-rich layered oxides.